Migraine aura: retracting particle-like waves in weakly susceptible cortex

M. A. Dahlem[1,2,3] and N. Hadjikhani[4,5]

[1]*Institut für Theoretische Physik, Technische Universität Berlin, Hardenbergstraße 36, 10623 Berlin, Germany*

[2]*Klinik für Neurologie II, Otto-von-Guericke-Universität Magdeburg, 39120 Magdeburg, Germany*

[3]*Leibniz Institute für Neurobiologie, 39118 Magdeburg, Germany*

[4]*Brain Mind Institute, EPFL, Lausanne, Switzerland*

[5]*Martinos Center for Biomedical Imaging, Massachusetts General Hospital, Harvard Medical School, Charlestown, MA 02129, USA*

Cortical spreading depression (SD) has been suggested to underlie visual migraine aura. Despite a precise match in speed, the spatio-temporal patterns of SD and aura symptoms on the cortical surface ordinarily differ in aspects of size and shape. We show that this mismatch is reconciled by utilizing that both pattern types bifurcate from an instability point of generic reaction-diffusion models. To classify these spatio-temporal pattern we suggest a susceptibility scale having the value $\sigma = 1$ at the instability point. We predict that human cortex is only weakly susceptible to SD ($\sigma < 1$), and support this prediction by directly matching visual aura symptoms with anatomical landmarks using fMRI retinotopic mapping. We discuss the increased dynamical repertoire of cortical tissue close to $\sigma = 1$, in particular, the resulting implications on migraine pharmacology that is hitherto tested in the regime ($\sigma \gg 1$), and potentially silent aura occurring below a second bifurcation point at $\sigma = 0$ on the susceptible scale.

1 Introduction

Migraine aura is a collection of transient neurological symptoms characterized by a gradual onset as the distinctive clinical feature. It may be classified into sensory and cognitive modalities. Visual aura predominate, usually consisting of a distortion in the visual field often characterized by an expanding zigzag pattern at the leading front and a scotoma in the back [1–6] (Fig. 1 (a)). Direct correlations between aura percepts and neural properties have been demonstrated, e. g., the typical zigzag patterns are reflected in reversed cortical feature maps[2,7,8]. While the pseudohallucinatory percept during the aura (visual or other) is specific from the affected sensory modality and is independent of etiology[9], the spatio-temporal course of aura progression is a clear signature of the underlying pathological process.

Reverse retinotopic mapping of aura symptoms reveals a constant propagation speed of about 3 mm/min on the cortical surface [1,6] (Fig. 1 (b)). The remarkable slow velocity fits with the pace of spreading depression (SD), a profound but transient all-or-none type process characterized by redistribution of ions across cell membranes and nearly complete neuronal depolarization[10,11]. This suggests that both phenomena rely on the same propagation mechanism[12].

Despite the precise match in speed of mapped aura symptoms and SD, both processes ordinarily differ in aspects of size and shape on the cortical surface. While SD waves usually invade the entire gray matter region and stop only at the border to white matter—at least if observed in the most prone brain regions, the hippocampus and neocortex of nonprimate mammals—migraine aura symptoms, in contrast, seem to be more spatially confined. This can be deduced from the

fact that visual symptoms often last not longer than 20 min corresponding to a distance of 60 mm, the length of the early visual areas located along the sulcus calcarine (Fig. 1). It is the central result of this article to show that this mismatch in size and shape between mapped aura symptoms and SD propagation may be reconciled by utilizing that both pattern types occur in a generic reaction-diffusion model but are separated by a bifurcation, that is, a sudden qualitative change in the spatio-temporal SD pattern after only a small smooth change made to cortical susceptibility to SD. Our predictions are supported by directly matching visual aura symptoms with anatomical landmarks using fMRI retinotopic mapping.

Our results lead us to the conclusion that SD in humans is much closer to a bifurcating instability point of pattern formation than in nonprimate mammals. From a synergetics point of view, the brain is in general viewed as a self-organizing pattern forming system that operates close to instability points[13]. In the case of migraine aura, the crucial instability point separates transient from sustained wave propagation. Being close to the instability point dramatically changes the dynamical repertoire. This factor, as will be discussed, should have severe implications on the design of migraine drug tests. Moreover, it may favor the hypothesis of the occurrence of silent aura in diagnosed forms of *migraine without aura*[14].

2 Results

The visual aura symptoms typically affect only a part, albeit large part, of a visual hemifield (VH). The affected area forms an expanding circular arc often centred close to the fovea. In Fig. 1

(a), a sequence of subsequent migraine aura "snapshots" visualizes the typical course of a visual disturbance in the right VH. The perimetric data is taken from Lashley[1] and the corresponding spatio-temporal pattern in the primary visual cortex (V1) is obtained by reversed retinotopic mapping (Fig. 1 (b)). The crescent pattern in the VH translates into a wave segment resembling a "particle-like wave"[15], as described in the next subsection. From this pattern, we can estimate an average length of the wave front of about 35 mm and a propagation speed of 3mm/min. Therefore, such a wave segment temporarily recruits a total of about 2100mm^2 cortical surface within 20 min into the depolarized SD state, that is, only approximately 1.7% of the surface of one human cortical hemisphere.

Susceptibility scale based on wave instabilities Transient and spatially confined waves were first suggested to cause aura symptoms in a descriptive mathematical model considering the motion of curves with free ends[16]. These curves represent segments of excitation fronts with two open ends, as shown in Fig. 1 (b). Furthermore, unstable—and thus also transient and spatially confined—waves, termed *particle-like waves* have been found and studied in the chemical Belousov-Zhabotinskii (BZ) reaction and their spatio-temporal dynamics are described by reaction-diffusion (RD) equations [15,17,18]. Particle-like wave propagation differs significantly from the current view of SD as a pattern engulfing posterior cortex (Fig. 1 (a)).

We suggest to introduce a macroscopic susceptibility scale σ to classify such spatio-temporal RD patterns in excitable media that are weakly susceptible to SD wave propagation. A two-point definition is used for calibrating this scale, whereby $\sigma = 1$ represents particle-like waves and

$\sigma = 0$ the propagation boundary (see Methods). The two points are defined each by such a bifurcation point. The value $\sigma = 1$ separates excitable media with capacity to propagate growing waves segments ($\sigma > 1$) from those where only retracting waves segments ($\sigma < 1$) occur. When susceptibility changes to a value below $\sigma = 0$, the amplitude of the wave decreases so that a wave segment not only retracts from its sides (decreasing length as indicated by green arrow heads in Fig. 2 (b)) but also its wave profile collapses (decreasing width).

The two bifurcation at $\sigma = 0$ and $\sigma = 1$ are generic in the sense that they apply to excitable media based on RD mechanisms irrespective of the particular model. In Fig. 2, generic spatio-temporal RD patterns are classified into four intervals based on a linear scale between the points $\sigma = 0$ and $\sigma = 1$. The linear scale and the locus of further bifurcation points on this scale depend on the specific RD model. We used the FitzHugh-Nagumo system (FHN) and fixed all parameters but the threshold β such that the experimentally observed re-entrant pattern of retinal SD, which performs a complex meandering[19], is obtained at $\sigma > 2$ (Methods)[20,21].

Four susceptibility intervals are relevant for reconciling the mismatch in size and shape between mapped aura symptoms and SD propagation. They are ordered by decreasing susceptibility: (a) ($\sigma > 1$): sustained waves, (b) ($1 > \sigma > 0$): retracting waves, (c) ($\sigma < 0$): collapsing waves, (d) ($\sigma < 2.2$): no spread.

The regime (a) has the highest susceptibility to spreading phenomena due to the lowest threshold values among the four intervals. The spatio-temporal patterns obtained in (a) show the typical course of SD waves observed in animal experiments. In particular, an SD wave, initiated at

the occipital pole and propagating in anterior direction, will eventually engulf the whole cortical surface. In this regime, wave segments with free open ends curl in to form rotors (spiral shaped waves), therefore the lower bound $\sigma = 1$ is called the rotor boundary (RB)[20]. RB is marked by the occurrence of particle-like waves. Adhering strictly to the definition of particle-like waves as a wave form with natural length and shape that will either grow or decay when perturbed, RB is wave size dependent[17]. In the limit of large wave segments (critical fingers[22,23]) susceptibility approaches a lower bound that is used as the defining point for calibrating σ.

In both the intervals (b) and (c) transient waves forms occur. In (b), the interval with higher susceptibility among (b) and (c), 2D wave segments with free open ends, such as shown in Fig. 1 (b), eventually disappear because open ends retract and thereby constantly reduce the instantaneous size of excitation. In susceptibility interval (c) the RD equations describe rather a process of facilitated diffusion than travelling wave processes in excitable media. For this reason, the boundary between (b) and (c) is called propagation boundary (PB)[20,23]. In (c), the pulse evolution, following an initial increase in the activator, is similar to passive diffusion only that the spatially elevated distribution collapses slower than without the activator reaction and this process can be directed, if the spatial distribution of activator and inhibitor are not symmetric. In regime (d), an initially imposed localized spatial distribution of the activator collapses without broadening (spreading boundary (SB)) because the reaction part provides a sink that decreases the activator faster than it is transported outwards by diffusion[24].

Effects of gyrification on RD waves Critical properties of RD waves such as retracting particle-like wave propagation in the weakly susceptibility domain $1>\sigma>0$ are modulated by the bending of the cortical surface. This can be deduced from experimental and theoretical[25–28] studies of the chemical BZ model systems of RD waves on curved surfaces in the regime of weakly excitable media. Weak excitability is not strictly defined but usually refers to values close to $\sigma=1$. In these systems, it is shown that propagation depends crucially on the geometric properties of the surface. As a consequence, we can predict that a correlation must exist between anatomical landmarks and the course of aura symptoms if migraine aura is caused by a RD process.

In this subsection, we consider the gross gyral morphology in relation to the typical aura onset, course and ending. But before, we refer to a particular curvature-induced phenomenon that provided a mechanism how wave segments can emerge in the first place. It was shown that the wave front can undergo a critical deformation above which propagation is blocked[29]. A broken wave front is needed to distinguish spatio-temporal pattern obtained in the susceptibility intervals ($\sigma>1$) and ($1>\sigma>0$). The evolution of closed wave fronts does not differ much until the front breaks open, for instance due to a local curvature-induced excitation block. Then the resulting open ends will either grow or retract if the susceptibility σ is in the interval ($\sigma>1$) and ($1>\sigma>0$), respectively.

If migraine aura is caused by retracting RD waves ($1>\sigma>0$) that are guided by anatomical landmarks, the main course of the neurological symptoms within different people can be similar, because many studies of human cytoarchitecture show that sensory and motor areas have some

relationship to the gross sulcal and gyral morphology. In some cases very precise correlations between sulci and functional entities could be demonstrated, most prominent is the calcarine sulcus (CS) as a landmark of the primary visual cortex (V1)[30]. Furthermore, the primary auditory cortex has a clear spatial relationship with Heschl's gyrus[31,32], and the motor cortex can be identified by the position of the central sulcus[33]. Yet a substantial interindividual and interhemisphere variability in both size and location of anatomical landmarks is observed[34], and major sulci and gyri are individually composed of smaller gyral folds and sulci indents, which provides a variability for individual local characteristics of the spatio-temporal aura symptoms.

Due to CS's precise landmark position of V1[30] its geometric properties are best suited for comparison with visual aura symptoms. Furthermore, its retinotopic mapping of visual input is well studied in human[35–38]. We therefore consider the gross morphology of CS and the relative position of V1 in relation to the typical onset, course and ending of crescent shaped visual aura as shown in Fig. 1.

Onset Most of the crescent shaped aura pattern start in one VH close to the fovea (center of gaze). The neural representation of the fovea is located at the occipital pole often extending about 10 mm onto the lateral convexity. CS is formed by the cuneus and lingual gyrus on the medial surface and runs forward to the corpus callosum. Approximately two-thirds of V1 lies within the CS walls [30]. A difference of 1° visual angle between the onset of aura symptoms and the fovea corresponds to a cortical distance of about 1cm (see Fig. 1) because of the large linear cortical magnification factor M (see Methods) close to the fovea. Therefore, the crescent aura symptoms

start near the entrance of CS.

Course Typical crescent pattern propagate along the horizontal hemimeridian (HM) towards the visual periphery. The pattern extends into both quadrants of the VH, which is a clear sign that it is caused in V1. V1 is the only of the early visual areas where the two quadrants of the VH are not split along HM[39]. Extrastriate visual cortical areas represent the two quadrants of VH in dorsal and ventral areas that are connected only close to the fovea. And the pattern is caused in early visual areas because orientation selective cells with moderate receptive field sizes are only found there. They represent the individual edges of the zigzag aura percept at the propagating front[8].

The locus of the neural representation of HM in V1 is near the fundus of CS. Individual aura reports show an asymmetric propagation to either the upper or lower visual field quadrant [1–3,6]. If the visual field defect falls behind in one visual quadrant, this could indicate that M is larger in this quadrant. In deed, anatomical data suggest that V1 proceeds farther anteriorly in the lingual gyrus[30,40], which suggests that more cortical surface is devoted to upper quadrant, however, fMRI data show that the dorsal and ventral compartments of V1 are at least similar in absolute extent measured in geodesic distance [38].

Ending Visual aura symptoms stop in the periphery of the VH. The extreme periphery of the VH is represented at the anterior boundary of V1 close to the T-shaped or sometimes Y-shaped junction of the CS and the medial part parieto-occipital sulcus. Such a junction might act as a diode being

transparent for wave propagation only in one direction, but not in the other. Critical properties of excitation waves on curved surfaces that lead to a curvature-dependent loss of excitability have been studied in BZ system[28].

The CS as a major sulci is composed of smaller gyral folds and sulci indents resulting in a complex surface. While the gross morphology of CS can determine the basic course of particle-like wave propagation, it is this individually complex surface that needs to be considered if precisely recorded perimetric data of visual aura progression are compared with anatomy. Furthermore, only rather sharp deformations of the cortical surface can directly induce a critical deformation in the wave front above which propagation is then blocked[29]. The effect of smaller gyral folds and sulci is considered in the next subsection.

fMRI retinotopy and perimetric aura data To investigate the effects of small gyrification pattern on RD waves, the 3D form of V1 and its retinotopic map was obtained by fMRI from a migraineur (PVV) who has made precise perimetric recordings of his visual aura[41]. In Fig. 3 (a), the right V1 is shown. Its color codes the azimuthal angle of the contralateral left VH by a half HVS (hue, value, saturation) color wheel, in counterclockwise direction from red (upper hemimeridian) via light green (HM) to cyan (lower hemimeridian). The rostral/caudal (r, c) and dorsal/ventral (d, v) directions are indicated by a cross.

The dorsal bank of the right CS is noticeable heavily ramified with small gyral folds and sulci indents. The progression pattern of the visual field defect in the lower visual quadrant shows accordingly a rather complex pattern. The spatial progression is marked in Fig. 3 (b) by drawing

with white lines the current position of the propagating field defect at one minute intervals within 24 minutes. The wave runs from minute 4 to 13 in the lower visual quadrant and this quadrant is mapped, as can be seen by the color code, onto the dorsal bank of CS. Partly the wave pulsates back and forth between 11-13 minute and eventually terminates in the lower end of this visual quadrant in an excitation block, but continues to propagate within the upper quadrant.

In Fig. 3 (c), the left V1 is shown with the color coding azimuthal angles of the contralateral right VH by the other half HVS color wheel, in counterclockwise direction from cyan (lower hemimeridian) via dark magenta (HM) to red (upper hemimeridian). Marked with white lines at one minute intervals, the spatial progression of the visual aura in the right VH is shown in Fig. 3 (d). As can be seen by the color code, the wave runs from minute 1 to 8 over a gyral crown (gc) as part of the cuneus. Between minute 8 to 15 the wave disappeared, but reappeared at minute 15 propagating upwards in the visual field for a duration lasting 12 minutes being approximately parallel to visual hemimeridians, i. e., running from the dorsal to the ventral bank of CS and ending on the anterior edge of the lingual gyrus.

3 Discussion

The crescent shaped aura pattern, as shown in Fig. 1 (a), is often reported [1–6] but the phenomenology of migraine aura is much richer as documented by the variety of illustrations and descriptions collected on the Migraine Aura Foundation website (www.migraine-aura.org). In a single migraine aura attack, migraineurs can also experience diverse visual, as well as sensory, motor and language

disturbances[42,43]. This variety clearly indicates that other areas beside early visual cortex can be affected, even cortical areas outside the occipital lobes, and it therefore seemingly supports the idea that the process causing the aura can engulf all of posterior cortex on its course, like a cortical SD wave observed in animal experiments.

Schematic drawings similar to Fig. 2 (a) illustrate engulfing spatio-temporal wave patterns. Such illustrations are found in modern textbooks of headache[44] and appeared first in Lauritzen's seminal paper spearheading the SD theory of migraine aura[45]. They became paradigmatic for migraine with aura. However, they might need to be revised, as we show.

The activity pattern causing crescent shaped aura is remarkably similar to a particle-like wave segment on the cortical surface (Fig. 1), a pattern that exists only in cortex being weakly susceptible to SD. Other factors also support the concept that human cortex is only weakly susceptible to SD, maybe foremost that susceptibility becomes the lower the higher up the species is in the phylogenetic tree. Another clear indication is that SD propagation is modulated by cortical morphology, as can be seen in Fig. 3. Similar pattern were also observed for the gyrencephalic feline brain[46], but there the primary SD wave engulfed the hemisphere and only succeeding secondary waves remained within the originating gyrus and were more fragmented. Since secondary waves run into partly refractory tissue, susceptibility to SD is decreased.

The engulfing wave pattern is originally motivated by SD propagating in the smooth cortex of rats and rabbits. It has been debated whether SD can occur in the highly convoluted cortex of humans, until spatial and temporal events were followed using high-field functional MRI [47]

demonstrating that at least eight characteristics of SD are present and the events are time-locked to percept onset of the aura in human cortex. However, the precise spatio-temporal course of the events is still ambiguous. Much of posterior cortex, including several retinotopically organized visual areas, showed simultaneous activation during much of the period of the aura, while the percept in the VHs is reported to be more spatially confined.

As already noted by Wilkinson[48] this mismatch in fMRI data and aura percept can be explained by at least two alternatives: (i) either SD engulfs all of posterior cortex. Then only a subset of this activation results in sensory awareness. Or (ii), the spread of the SD wave is, in contrast to the fMRI data, more limited in extent. Then the rest of the observed activation in adjacent cortical areas represents synaptic activation through feed-forward and feedback circuitry. While (i) is in agreement with observed cortical SD wave patterns in animals, it opens up questions about the nature of the often reported limitation to spatially confined crescent-shaped visual field defects. In (ii) spatially confined SD waves causing corresponding field defects are simply postulated[48].

If SD in human is more limited in extent, the mismatch with animal data needs to be addressed. To reconcile this, we provide a theoretical framework, which is, moreover, of practical use to both experimental neuroscientists and clinicians. We propose a susceptibility scale σ based on nonlinear bifurcation analysis. Not unlike the Celsius temperature scale, the term *susceptibility to SD* is made a precise scale by a two-point definition, i. e., two macroscopically observable cortical states at which a phase transition in SD pattern formation occurs. The relevance and applicability of this scale is described in the following.

The weakly susceptible state ($1>\sigma>0$) of human cortex to SD can be achieved in experimental migraine models if the tissue is preconditioned reducing excitability towards the gray marked regime in Fig. 2. The procedure to find this regime experimentally is described in the Methods section for retinal SD. Retinal SD is accompanied with an intrinsic optical signal that makes precise spatio-temporal recordings of the evolutionary SD pattern possible. Similar precise spatio-temporal recordings have been made in cortex using a fluorescent, voltage-sensitive dye [49].

We predict that effects of antimigraine drugs depend on the susceptibility range they are tested in, because the dynamical behavior of a nonlinear system changes drastically when crossing a bifurcation point. Antimigraine drugs tests and tests to unravel the mechanism of SD in retina[50–52] have been performed far away from the regime ($1>\sigma>0$). This can be shown, by precisely measuring in this system the complex meandering pattern of spiral SD[19]. On the σ scale, obtained from the generic FHN model, these pattern occur above $\sigma>2$ and are separated by two further bifurcations [21]. In general, SD experiments are performed in the most prone tissue regions where SD can more easily be observed. This might remind one at Watzlawick's man searching for his keys under the streetlight rather than where he lost them[53].

Furthermore, our results supports the idea that SD could activate the trigeminovascular system that generates and maintains migraine pain [54] even in diagnosed forms of *migraine without aura*. For susceptibility values below the weakly susceptible regime, the model predicts spatio-temporal SD pattern that do not break away from an initially restricted focus. We can draw a direct analogy to clinically silent epilepsy caused by interictal activity that does not break away from a

focus. Likewise, previously proposed silent aura, in which "some migraineurs exhibit blood flow 'fingerprints' of CSD [cortical SD] and aura but are subjectively unaware that the phenomenon is propagating"[14], may be explained by localized SD patterns occurring at the one end of the increased dynamical repertoire that emerges if being close to a bifurcation.

4 Methods

Susceptibility scale in experimental and mathematical models A two-point definition is used for calibrating the newly introduced susceptibility scale σ. These two points are macroscopically observable states. We shortly describe an experimental procedure to measure such states. A precise determination of these two states in an animal model of SD is, however, beyond the scope of our proof of concept. RB ($\sigma = 1$) can be obtained by changing the tissue excitability until open wave segments stop curling in to form reentrant SD waves with freely rotating open ends forming two centers (spiral SD)[55]. For instance, to obtain an SD wave segment in submerged retina (for details, see Ref. [19]), an initially closed circular SD wave front can be broken (at a diameter of about 0.75 mm) by local application of 0.5 ml Ringer solution through a pipette (tip diameter 0.5 mm) containing a tenfold raised Mg^{2+} concentration (10 mM) (Fig. 4).

In Fig. 5 a retinal SD wave segment is shown that evolves into a double spiral ($\sigma > 1$). The mathematical model (see below) predicts that after crossing $\sigma = 1$ (RB), the open ends of the wave segments retract (direction indicated by green arrows in Fig. 5) and the SD wave eventually vanishes. The Mg^{2+} concentration in Ringer at which this transition occurs is in this experimental

set-up difficult to determined, because the initial raise in Mg^{2+} needed to break the circular wave front cannot sufficiently fast be washed out. However, it is known that lowering calcium concentration to 0.5 mM and increasing magnesium to 2.0 mM turns the tissue absolute refractory to SD[56], which corresponds to the regime $\sigma < 0$ and giving a lower bound of $\sigma = 0$.

The locus of RB as a function of excitability represents a critical perturbation threshold[17], separating an attractor characterized by spiral waves from an attractor characterized by the uniform physiological steady state of the cortex. Such a threshold (RB) must exist if spiral SD waves occur in the tissue and therefore the existence of RB is independent of the particular model that describes the pattern formation process. The locus of PB can be obtain similarly by decreasing further the tissue excitability until reentrant SD waves collapse even if their open ends are attached to either the border of the retina or a lesion (circling SD [57]).

In mathematical models of SD, the critical points RB and PB are found by bifurcation analysis. Some SD models investigate the local ignition of SD by mathematical models of single cells and their surrounding compartments[58,59]. Those models lack a spatial extension beyond the cell size. They cannot yet address the clinically relevant question whether a local ignition stays confined or breaks away but such microscopic models help to understand the pathophysiological mechanism of SD and if they will be extended by a spatial coupling, such as a diffusion term, also those models become accessible to the bifurcation analysis described in the following.

We exemplify with a standard RD scheme of activator-inhibitor type the determination of the location of RB and PB in the parameter space of this model and how to obtain from a parameter

value the susceptibility scale σ. By choosing an activator-inhibitor type SD model, we assume that all quantities with a positive feedback loop can be lumped together, such as extracellular potassium concentration $[K^+]_o$ and inward currents[60,61]. They become a single *activator* variable u. The rate of change in u is given by a single nonlinear reaction rate f. Likewise, a single inhibitor variable v represents the recovery processes with reaction rate g. Processes represented by inhibitor kinetics are, amongst others, the effective regulation of $[K^+]_o$ by the neuron's Na^+-K^+ ion pump and the glia-endothelial system. The general form of a RD equation is then

$$\begin{aligned} \frac{\partial u}{\partial t} &= f(u,v) + D\nabla^2 u \\ \frac{\partial v}{\partial t} &= g(u,v), \end{aligned} \tag{1}$$

where the term $D\nabla^2 u$ represents the spatial coupling of the local dynamics by diffusion of u with diffusion coefficient D.

The variety of macroscopic RD pattern in u and v, such as spirals and retracting waves, is largely independent of the specific reaction rates $f(u,v)$ and $g(u,v)$, as long as the local dynamics ($D = 0$) show all-or-none type behavior. To obtain the scale σ shown in Fig. 2 we chose the FitzHugh-Nagumo equations $f(u,v) = u - u^3/3 - v$ and $g(u,v) = (u + \beta)/25$, where β is a threshold parameter that selects the pattern. In this system, particle-like waves can be stabilized with a control term that changes β as a linear function of wave size, a feedback mechanism first proposed for chemical BZ waves[17]. At $\beta_{RB} = 1.34$ the limit of large particle-like waves is reached (critical fingers [22,23]). The propagation boundary is found by transforming Eqs. 1 into a co-moving frame and determine the largest value $\beta_{PB} = 1.39$ for which bounded profile solutions exist [24]. The

susceptibility scale, as a linear function of β with the defining points $\sigma = 1$ and $\sigma = 0$ corresponding to RB and PB, respectively, is then obtained by

$$\sigma(\beta) = \frac{\beta - \beta_{RB}}{\beta_{RB} - \beta_{PB}} + 1. \tag{2}$$

This formula is independent on the specific choice of β as a parameter to change excitability, e. g., in an experimental system β_{RB} and β_{PB} could be taken as the concentration of Mg^{2+} as described above. If more then on parameter is accessible to change tissue excitability a shortest, i.e., metrical, distance between RB and PB can be defined via pharmacokinetic-pharmacodynamic models[24].

Perimetric recordings and retinotopic mapping The perimetric data shown in Fig. 1 were taken from Lashley's precise drawings published in 1941[1]. The radial coordinate (eccentricity) of the crescent shaped aura pattern in the right VH was calibrated assuming the blind spot (not shown in Fig. 1) at 10°. The eccentricity is then obtained assuming the percept is projected to a flat tangent plane with respect to the center of the spherical visual field. This tangent plane serves as the canvas to draw the aura percept. The azimuthal coordinate can be taken directly form the drawing in the tangent plane.

The flat retinotopic map in Fig. 1 (b) was created by using the monopole map, that is, the complex logarithm $w = A \log(z/E_2 + 1)$ with the cortical magnification parameter $E_2 = 0.75$ and $A = 17.3$ adjusted to human data [62]. The complex coordinates z and w describe locations in the visual field and in the cortical domain, respectively. The magnitude of z is the visual eccentricity θ and its argument ϕ is the azimuth ($z = \theta e^{i\phi}$). The real and complex parts of w are Cartesian coordinates on the cortical surface. From the monopole map it follows that the linear cortical

magnification factor along HM is $M(\theta) = \frac{A}{\theta + E_2}$.

The perimetric data shown in Fig. 3 were provided by a participant (PVV) who fulfills the International Headache Society criteria for the diagnosis of migraine with aura. As a research engineer he trained himself to make precise recordings during his migraine with aura attacks and documented over 350 aura episodes over 10 years [41]. To compare the topography of the visual aura with anatomical landmarks of the cortex, the retinotopic organization in the visual cortex was obtained with functional magnetic resonance imaging (fMRI). The data were acquired in a 3-Tesla scanner, using echoplanar imaging as described in Refs. [47,63]. All procedures were approved by MGH IRB.

Acknowledgement

The authors want to acknowledge PVV for his active participation in data collection and are indebted to Jochem Rieger, Jan Tusch, Roland Aust, and Josh Snyder for technical assistance, and to Gerald Hiller for comments on the manuscript. MAD was supported by the Deutsche Forschungsgemeinschaft (DA 602/1-1 and SFB 555). NH was supported by NIH grant 5PO1NS 35611-09.

1. Lashley, K. Patterns of cerebral integration indicated by scotomas of migraine. *Arch. Neurol. Psychiatry* **46**, 331–339 (1941).

2. Richards, W. The fortification illusions of migraines. *Sci. Am.* **224**, 88–96 (1971).

3. Pöppel, E. Fortification illusion during an attack of ophthalmic migraine. Implications for the

354 human visual cortex. *Naturwissenschaften* **60**, 554–555 (1973).

355 4. Jung, R. [Translocation of cortical migraine phosphenes through eye movements and vestibu-
356 lar stimulation]. *Neuropsychologia* **17**, 173–185 (1979).

357 5. Hubel, D. H. *Eye, Brain, and Vision* (W H Freeman & Co, NewYork, 1988).

358 6. Grüsser, O.-J. Migraine phosphenes and the retino-cortical magnification factor. *Vision Re-*
359 *search* **35**, 1125–1134 (1995).

360 7. Schwartz, E. L. A quantitative model of the functional architecture of human striate cortex
361 with application to visual illusion and cortical texture analysis. *Biol Cybern* **37**, 63–76 (1980).

362 8. Dahlem, M. A., Engelmann, R., Löwel, S. & Müller, S. C. Does the migraine aura reflect
363 cortical organization. *Eur. J. Neurosci.* **12**, 767–770 (2000).

364 9. ffytche, D. H. & Howard, R. J. The perceptual consequences of visual loss: 'positive' patholo-
365 gies of vision. *Brain* **122**, 1247–1260 (1999).

366 10. Leão, A. A. P. Spreading depression of activity in the cerebral cortex. *J. Neurophysiol.* **7**,
367 359–390 (1944).

368 11. Somjen, G. G. Mechanisms of spreading depression and hypoxic spreading depression-like
369 depolarization. *Physiol. Rev.* **81**, 1065–1096 (2001).

370 12. Milner, P. M. Note on a possible correspondence between the scotomas of migraine and
371 spreading depression of Leão. *Electroencephalogr. Clin. Neurophysiol.* **10**, 705 (1958).

13. Haken, H. *Synergetics, An Introduction* (Springer, Berlin, 1983), 3 edn.

14. Moskowitz, M. A. Defining a pathway to discovery from bench to bedside: the trigeminovascular system and sensitization. *Headache* **48**, 688–690 (2008).

15. Sakurai, T., Mihaliuk, E., Chirila, F. & Showalter, K. Design and control of wave propagation patterns in excitable media. *Science* **296**, 2009–2012 (2002).

16. Dahlem, M. A. & Müller, S. C. Migraine aura dynamics after reverse retinotopic mapping of weak excitation waves in the primary visual cortex. *Biol. Cybern.* **88**, 419–424 (2003).

17. Mihaliuk, E., Sakurai, T., Chirila, F. & Showalter, K. Feedback stabilization of unstable propagating waves. *Phys. Rev. E* **65**, 065602 (2002).

18. Mikhailov, A. S. & Showalter, K. Control of waves, patterns and turbulence in chemical systems. *Phys. Rep.* **425**, 79–194 (2006).

19. Dahlem, M. A. & Müller, S. C. Self-induced splitting of spiral-shaped spreading depression waves in chicken retina. *Exp. Brain Res.* **115**, 319–324 (1997).

20. Winfree, A. T. Varieties of spiral wave behaviour: An experimentalist's approach to the theory of excitable media. *Chaos* **1**, 303–334 (1991).

21. Dahlem, M. A. & Müller, S. C. Reaction-diffusion waves in neuronal tissue and the window of cortical excitability. *Ann. Phys.* **13**, 442–449 (2004).

22. Karma, A. Universal limit of spiral wave propagation in excitable media. *Phys. Rev. Lett.* **66**, 2274–2277 (1991).

391 23. Hakim, V. & Karma, A. Theory of spiral wave dynamics in weakly excitable media: asymp-
392 totic reduction to a kinematic model and applications. *Phys. Rev. E* **60**, 5073–5105 (1999).

393 24. Dahlem, M. A., Schneider, F. M. & Schöll, E. Efficient control of transient wave forms to
394 prevent spreading depolarizations. *J. Theo. Biol.* **251**, 202–209 (2008).

395 25. Maselko, J. & Showalter, K. Chemical waves on spherical surfaces. *Nature* **339**, 609–611
396 (1989). 10.1038/339609a0.

397 26. Davydov, V. A., Zykov, V. S. & Mikhailov, A. S. Kinematics of autowave structures in ex-
398 citable media. *Sov. Phys. Usp.* **34**, 665–684 (1991).

399 27. Davydov, V. A., Manz, N., Steinbock, O., Zykov, V. S. & Müller, S. C. Excitation fronts on a
400 periodically modulated curved surface. *Phys. Rev. Lett.* **85**, 868–871 (2000).

401 28. Davydov, V. A., Manz, N., Steinbock, O. & Müller, S. C. Critical properties of excitation
402 waves on curved surfaces: Curvature-dependent loss of excitability. *Europhys. Lett.* **59**, 344–
403 350 (2002).

404 29. Davydov, V. A., Morozov, V. G. & Davydov, N. V. Critical properties of autowaves propagat-
405 ing on deformed cylindrical surfaces. *Physics Letters A* **307**, 265–268 (2003).

406 30. Andrews, T. J., Halpern, S. D. & Purves, D. Correlated size variations in human visual cortex,
407 lateral geniculate nucleus, and optic tract. *J. Neurosci* **17**, 2859–2868 (1997).

31. Gaschler-Markefski, B. *et al.* Statistical methods in functional magnetic resonance imaging with respect to nonstationary time-series: auditory cortex activity. *Magn. Reson. Med.* **38**, 811–820 (1997).

32. Rademacher, J. *et al.* Probabilistic mapping and volume measurement of human primary auditory cortex. *Neuroimage* **13**, 669–683 (2001).

33. Lotze, M. *et al.* fMRI evaluation of somatotopic representation in human primary motor cortex. *Neuroimage* **11**, 473–481 (2000).

34. Roland, P. E. & Zilles, K. Structural divisions and functional fields in the human cerebral cortex. *Brain Res. Brain Res. Rev.* **26**, 87–105 (1998).

35. Engel, S. A. *et al.* fMRI of human visual cortex. *Nature* **369**, 525 (1994).

36. Sereno, M. I. *et al.* Borders of multiple visual areas in humans revealed by functional magnetic resonance imaging. *Science* **268**, 889–893 (1995).

37. Engel, S. A., Glover, G. H. & Wandell, B. A. Retinotopic organization in human visual cortex and the spatial precision of functional MRI. *Cereb. Cortex* **7**, 181–192 (1997).

38. Qiu, A. *et al.* Estimating linear cortical magnification in human primary visual cortex via dynamic programming. *Neuroimage* **31**, 125–138 (2006).

39. Polimeni, J. R., Balasubramanian, M. & Schwartz, E. L. Multi-area visuotopic map complexes in macaque striate and extra-striate cortex. *Vision research* **46**, 3336–3359 (2006). Published online July 10, 2006.

427 40. Stensaas, S. S., Eddington, D. K. & Dobelle, W. H. The topography and variability of the
428 primary visual cortex in man. *J. Neurosurg.* **40**, 747–755 (1974).

429 41. VanValkenburgh, P. Evidence indicating that pre-migraine csd can begin in either v1 or v2,
430 and cross a border into the other. *Journal of Vision* **5**, 90 (2005).

431 42. Russell, M. B. & Olesen, J. A nosographic analysis of the migraine aura in a general popula-
432 tion. *Brain* **119**, 355–361 (1996).

433 43. Vincent, M. & Hadjikhani, N. Migraine aura and related phenomena: beyond scotomata and
434 scintillations. *Cephalalgia* **27**, 1368–1377 (2007).

435 44. Silberstein, S. D., Stiles, A. & Young, W. B. (eds.) *Atlas of Migraine and Other Headaches*
436 (Taylor & Francis, London, 2005).

437 45. Lauritzen, M. Pathophysiology of the migraine aura. The spreading depression theory. *Brain*
438 **117**, 199–210 (1994).

439 46. James, M. F. *et al.* Cortical spreading depression in the gyrencephalic feline brain studied by
440 magnetic resonance imaging. *J. Physiol. (Lond.)* **519 Pt 2**, 415–425 (1999).

441 47. Hadjikhani, N. *et al.* Mechanisms of migraine aura revealed by functional MRI in human
442 visual cortex. *Proc. Natl. Acad. Sci. USA* **98**, 4687–4692 (2001).

443 48. Wilkinson, F. Auras and other hallucinations: windows on the visual brain. *Prog. Brain Res.*
444 **144**, 305–320 (2004).

445 49. Farkas, E., Pratt, R., Sengpiel, F. & Obrenovitch, T. P. Direct, live imaging of cortical spread-
446 ing depression and anoxic depolarisation using a fluorescent, voltage-sensitive dye. *J. Cereb.*
447 *Blood Flow Metab.* **28**, 251–262 (2008).

448 50. Wiedemann, M., de Lima, V. M. & Hanke, W. Effects of antimigraine drugs on retinal spread-
449 ing depression. *Naunyn Schmiedebergs Arch. Pharmacol.* **353**, 552–556 (1996).

450 51. Brand, S., Fernandes de Lima, V. M. & Hanke, W. Pharmacological modulation of the refrac-
451 tory period of retinal spreading depression. *Naunyn Schmiedebergs Arch. Pharmacol.* **357**,
452 419–425 (1998).

453 52. Scheller, D., Tegtmeier, F. & Schlue, W. R. Dose-dependent effects of tetraethylammonium
454 on circling spreading depressions in chicken retina. *J. Neurosci. Res.* **51**, 85–89 (1998).

455 53. Watzlawick, P. *The situation is hopeless, but not serious (The pursuit of unhappiness)* (W. W.
456 Norton & Company, 1993).

457 54. Sanchez-Del-Rio, M., Reuter, U. & Moskowitz, M. A. New insights into migraine pathophys-
458 iology. *Curr. Opin. Neurol.* **19**, 294–298 (2006).

459 55. Gorelova, N. A. & Bures, J. Spiral waves of spreading depression in the isolated chicken
460 retina. *J. Neurobiol.* **14**, 353–363 (1983).

461 56. Rodrigues, P. S., Guimarães, A. P., de Azeredo, F. A. & Martins-Ferreira, H. Involvement of
462 GABA and ACh in retinal spreading depression: effects of ”low calcium-high magnesium”
463 solutions. *Exp. Brain Res.* **73**, 659–664 (1988).

57. Martins-Ferreira, H., De Oliveira Castro, G., Struchiner, C. J. & Rodrigues, P. S. Circling spreading depression in isolated chick retina. *J Neurophysiol* **37**, 773–784 (1974).

58. Kager, H., Wadman, W. J. & Somjen, G. G. Simulated seizures and spreading depression in a neuron model incorporating interstitial space and ion concentrations. *J. Neurophysiol.* **84**, 495–512 (2000).

59. Makarova, J., Ibarz, J. M., Canals, S. & Herreras, O. A steady-state model of spreading depression predicts the importance of an unknown conductance in specific dendritic domains. *Biophys. J.* **92**, 4216–4232 (2007).

60. Grafstein, B. Locus of propagation of spreading cortical depression. *J Neurophysiol* **19**, 308–316 (1956).

61. Müller, M. & Somjen, G. G. Na^+ dependence and the role of glutamate receptors and Na^+ channels in ion fluxes during hypoxia of rat hippocampal slices. *J. Neurophysiol.* **84**, 1869–1880 (2000).

62. Horton, J. C. & Hoyt, W. F. The representation of the visual field in human striate cortex. A revision of the classic Holmes map. *Arch Ophthalmol* **109**, 816–824 (1991).

63. Tootell, R. B. H., Hadjikhani, N. K., Mendola, J. D., Marrett, S. & Dale, A. M. From retinotopy to recognition: fmri in human visual cortex. *Trends in Cognitive Sciences* **2**, 174–183 (1998).

Figure 1 (a) Right visual hemifield (dotted polar grid) with five subsequent sketched "snapshots" of a traveling visual migraine aura symptom in the shape of a crescent pattern. Numbers inside the scotom gives the time passed (in minutes) since first occurrence. (b) Visual field disturbance shown by reversed retinotopic mapping.

Figure 2 Schematic view of the spatio-temporal course of a reaction-diffusion wave for different tissue susceptibility values σ: wave front (red), recovery phase (yellow), blue arrows indicate normal velocity, future location is dashed (red). (a) sustained wave, (b) retracting wave, indicated by green arrow heads, (c) collapsing wave, (d) no spread. The gray σ interval is defined as weakly susceptible.

Figure 3 3D form of primary visual cortex (V1). The representation of the azimuthal coordinate of the two visual hemifields (VH) is given by the HVS (hue, value, saturation) color wheel: (a) right V1 (b) left VH (c) left V1 (d) right HV. The current position of the visual field defect, occurring during two different migraine aura attacks and each exclusively in one HV, are indicated by white lines, with numbers denoting the time in minutes after onset.

Figure 4 Creation of an SD wave segment with free open ends in submerged retina. (a) Mechanical stimulation with sharp glass needle s, (b) circular SD wave evolves, (c)-(d) local application of Mg^{2+} via pipette p, (e) wave propagation is locally blocked and consequently SD front brakes open and curls in to form a spiral at the lower open end, while the upper open end is guided by the Mg^{2+}-pipette to the border of the retina where it attaches.

Figure 5 Retinal SD wave segment propagating (blue arrows) with free open ends that grow (red arrow) and therefore curl in to form a double spiral. At lower susceptibility values, RD models of SD predict that open ends retract (green arrows) and the wave vanishes.

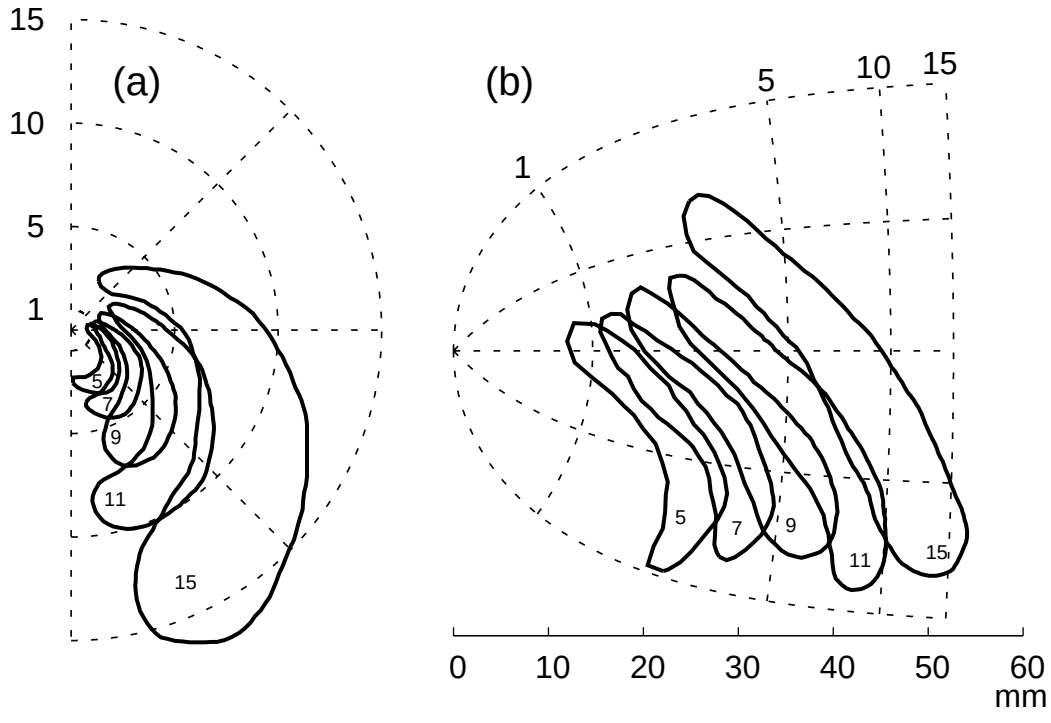
(a)
(b)
15
10
5
1
5
7
9
11
15
0
10
20
30
40
50
60
mm

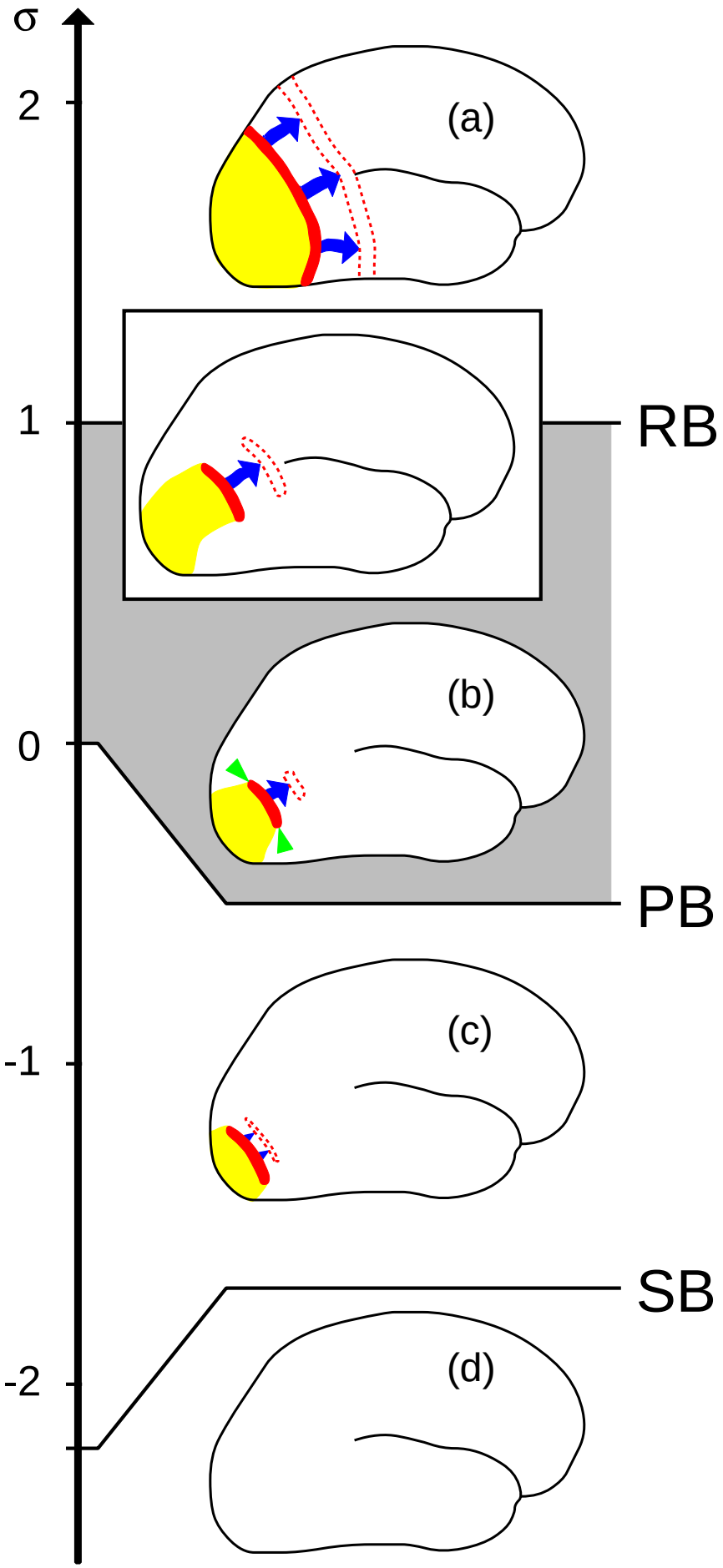
σ
2
1
0
-1
-2
(a)
(b)
(c)
(d)
RB
PB
SB

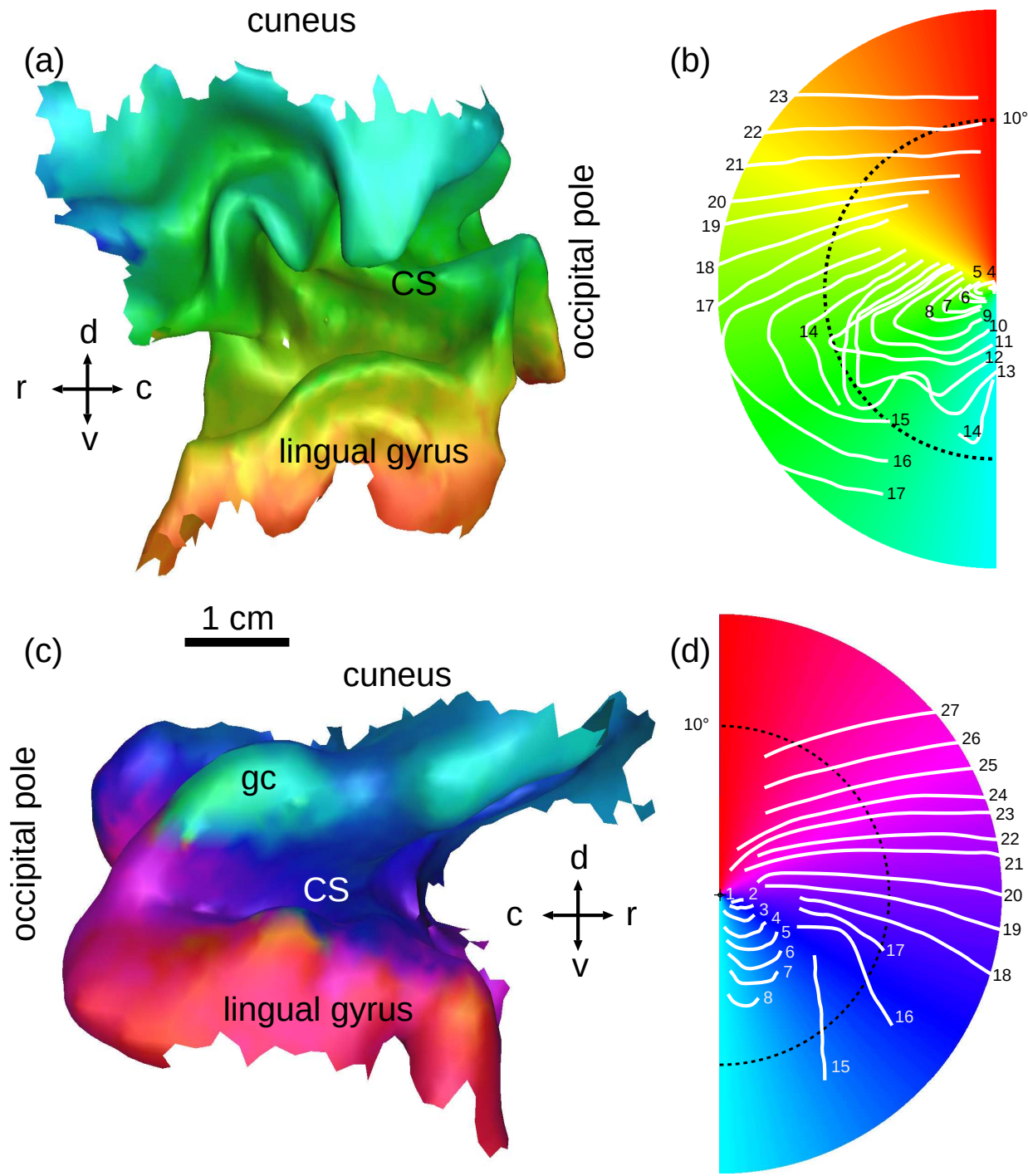
cuneus
(a)
occipital pole
CS
d
r
c
v
lingual gyrus
(b)
10°
23
22
21
20
19
18
17
5 4
6
7
8
9
10
11
12
13
14
15
14
16
17
1 cm
(c)
cuneus
occipital pole
gc
CS
d
c
r
v
lingual gyrus
(d)
10°
27
26
25
24
23
22
21
20
19
18
1
2
3
4
5
6
7
8
17
16
15

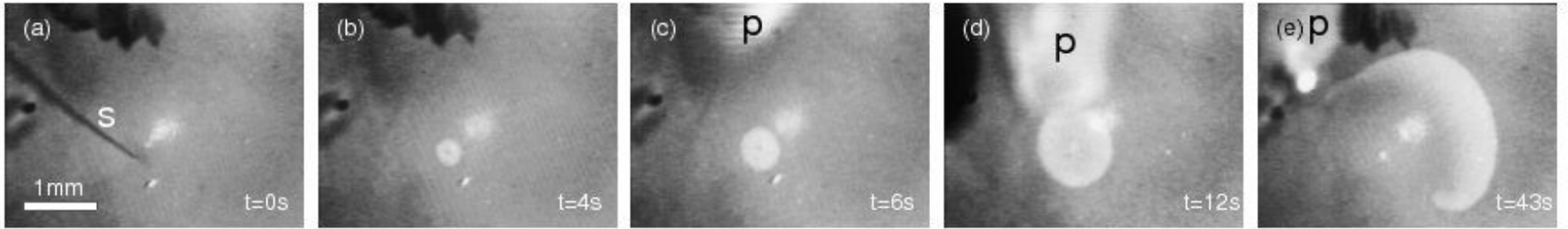
(a)
s
1mm
t=0s
(b)
t=4s
(c)
p
t=6s
(d)
p
t=12s
(e)
p
t=43s

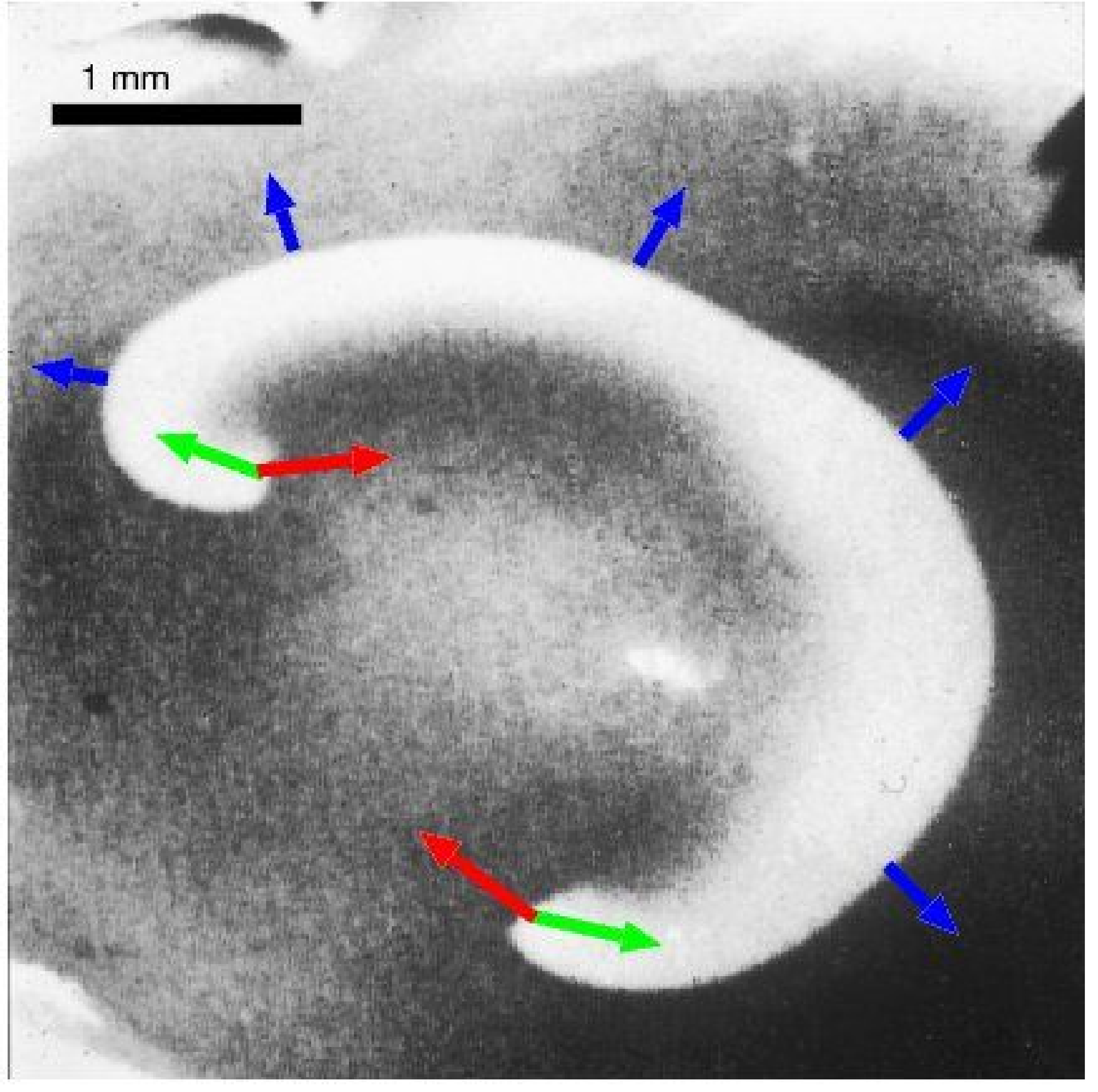
1 mm